

DFT Calculation, ADME/T and Molecular Docking Approach of Methyl 2-oxo-1,2-dihydrofuro[3,4-d] pyrimidine-3(4H)carboxylate

Gühergül Uluçam*

Chemistry Department, Faculty of Science, Trakya University, 22030 Edirne, Turkey.

*Corresponding author: Gühergül Uluçam, email: gulergul@trakya.edu.tr; Phone: +90 284 2351105; Fax: +90 284 2351198

Received March 7th, 2023; Accepted August 3rd, 2023.

DOI: <http://dx.doi.org/10.29356/jmcs.v68i3.1995>

Abstract. The optimized geometry of methyl 2-oxo-1,2-dihydrofuro[3,4-d] pyrimidine-3(4H) carboxylate (FP) was determined by density functional theory calculations. Geometric properties of FP such as bond length, bond angle, dihedral bond angle, and HOMO-LUMO energies in the gas phase were calculated by using the Gaussian program. Delocalization of the molecule's charge was analyzed using Mulliken Population Analysis (MPA) and Natural Population Analysis (NPA) approaches. Electrophilic and nucleophilic regions of FP were identified by drawing a molecular electrostatic potential map. NMR and FTIR spectra were calculated with the B3LYP and 6-311++G (2d, p) basis set and a detailed FTIR analysis was performed by using the VEDA program. To determine the consistency of the calculated NMR and FTIR spectra, they were compared with their corresponding experimental NMR and FTIR spectra. Molecular insertion studies of FP with six different cancer proteins were analyzed and their interactions were evaluated. Data on the pharmacokinetics and drug affinity of FP were obtained through the Swiss ADME and ADMET programs.

Keywords: Dihydrofuro [3,4-d] pyrimidine; DFT/B3LYP; molecular docking; swiss ADME; ADMET.

Resumen. Se optimizó la geometría del metil 2-oxo-1,2-dihidrofuro[3,4-d] pirimidina-3(4H) carboxilato (FP) por medio de la teoría de funcionales de la densidad. Utilizando el programa Gaussian, se calcularon en fase gas las propiedades geométricas del FP como longitudes de enlace, ángulos de enlace, ángulos diedros, y la diferencia de energías entre HOMO y LUMO. Se analizó la deslocalización de la carga en la molécula utilizando los análisis de población de Mulliken (MPA) y de población natural (NPA). Se identificaron las regiones electrofilicas y nucleofilicas mediante mapas del potencial electrostático molecular. Utilizando el funcional B3LYP y la base 6-311++G (2d, p) se calcularon los espectros de NMR y FTIR; se realizó un análisis detallado de los espectros de FTIR utilizando el programa VEDA. Para determinar la confiabilidad de los espectros calculados de NMR y FTIR, se compararon con los resultados experimentales. Se analizaron estudios de inserción molecular del FP a seis diferentes proteínas involucradas en cáncer para determinar sus interacciones. Utilizando los programas Swiss ADME y ADMET se determinaron la farmacocinética y la afinidad del FP.

Palabras clave: Dihidrofuro [3,4-d] pirimidina; DFT/B3LYP; acoplamiento molecular; Swiss ADME; ADMET.

Introduction

Pyrimidine, an aromatic heterocyclic compound containing nitrogen, is found in the structure of DNA and RNA, which are important for life. Synthesized pyrimidine-derived compounds can be used in many areas due to their features such as antifungal, anti-tumor, anti-inflammatory, anti-viral, anti-bacterial, anti-proliferative, anti-Alzheimer's, anti-tuberculosis, anti- β -glucuronidase, anti-HIV and diuretic [1-10]. Also, some cancer drugs like Xeloda [11], cytarabine [12] and gemcitabine [13], 5-fluorouracil [14] contain pyrimidine as the main component. Furopyrimidine compounds are synthesized by forming a pyrimidine ring next to the furan ring by various reactions. These compounds have biological properties similar to pyrimidines, which have been the subject of many studies in recent years [15-17]. It can be said that there is not much literature on quantum chemical calculations, molecular docking, ADME, and ADMET for furopyrimidine derivative compounds. For this purpose, methyl 2-oxo-1,2-dihydrofuro[3,4-d] pyrimidine-3(4H) carboxylate (FP) was first optimized using density functional theory (DFT). Bond angles, dihedral angles, bond lengths, dipole moments, molecular electrostatic potential map (MEP), highest occupied molecular orbital (HOMO), and lowest unoccupied molecular orbital (LUMO) of FP were obtained with the Gaussian G09w package program [18]. Then, the calculated spectrum values of FTIR and NMR were compared with the experimental spectrum values reported by Yilmaz et al. [19]. Finally, the biopotential of FP was evaluated by molecular docking with six different cancer proteins. Data on the pharmacokinetics and drug affinity of FP were obtained through the Swiss ADME [20] and ADMET programs [21].

Theoretical method

Geometric calculations and molecular configuration of the FP were performed in the Gaussian G09w package program with the 6-311++G (2d, p) basis set using B3LYP [22-24]. MAP and FMO were also calculated by the same method. The gauge invariant atomic orbitals (GIAO) method was used for ^1H and ^{13}C NMR. Since the experimental data were obtained in dimethylsulphoxide (DMSO), theoretical calculations were made in DMSO for comparison, and the solvent effect on the chemical shift value was also investigated by calculating NMR in the gas phase. The calculated IR vibration frequencies are multiplied by the correction factor 0.9613 which provides the best agreement between the theoretical data and the experimental FTIR frequencies for B3LYP/6-31G(d) method [24]. A detailed potential energy distribution (PED) analysis was also performed using the VEDA program. The visualization of all data was carried out in GaussView 5.0 [25-27].

Molecular docking

Since many *in vivo* and *in vitro* experiments are required, it is very difficult to determine whether the synthesized compounds have biological effects. Molecular docking calculation of ligand-receptor interactions provides easier information about the bioactivity of the compound [28-31]. The best ligand-receptor interaction can be examined by choosing the lowest energy interaction among the molecular docking results. Molecular docking studies were performed with Auto Dock Tools 1. 5. 6. [32,33]. Molecular docking FP with various cancer proteins, namely brain cancer, breast cancer, gastric cancer, liver cancer, lung cancer, and skin cancer [34-39]. The 3D crystal structure of cancer proteins was taken from Protein Data Bank (Brain Cancer Protein PDB ID: 1QHT, [40] Breast Cancer Protein PDB ID:1JNX [41], Gastric Cancer Protein PDB ID:1BJ7 [42], Liver Cancer Protein PDB ID:3WZE [43], Lung Cancer Protein PDB ID:2ITO [44], Skin Cancer Protein PDB ID:2VCJ [45]. Water molecules were removed, and polar hydrogens and Kollman United charges were added as the biomolecules were prepared for docking. The FP molecule was prepared for docking by minimizing its energy at the Gaussian 09w program [18]. Partial Charles of FP was calculated by Geistenger Method. The spacing between grid points was 0.375 Å. Autodock docking studies were examined by using the Lamarckian Genetic Algorithm (LGA). As a result of the calculations, the lowest energy interaction was selected, and the results were interpreted. All FP-biomolecule interactions were

illustrated using Pymol and Chimera software [46-48]. LigPlot+ v.1.4.5 software was used to show the H bonds in detail [49].

Swiss ADME and ADMET Lab

It is important to evaluate the bioavailability of compounds using computer-based programs for the discovery of new drugs. Compounds can be classified as drug-like and non-drug-like according to the Lipinski rule [50]. Physicochemical and pharmacokinetic properties of FP were obtained using the Swiss ADME free website <http://www.swissadme.ch/index.php> (Swiss Institute of Bioinformatics, Switzerland) [20]. ADMET (absorption, distribution, metabolism, elimination, toxicity) is an important part of drug discovery and provides information about the drug's behaviour in metabolism. ADMET properties of FP were obtained using the online ADMET database, <https://admetmesh.scbdd.com/service/screening/molecule> [51].

Results and discussion

Molecular geometry

Molecular geometry is defined as a three-dimensional arrangement of atoms in a molecule. According to the differences in the positions and orientations of the atoms, a lot of conformations can be determined for a compound. Each different conformation affects the energy of the molecule, its physical and chemical properties, its reactivity, and its interaction with other molecules [52]. The most stable optimized geometry of the FP at its minimum energy level obtained by DFT calculations is shown in Fig. 1.

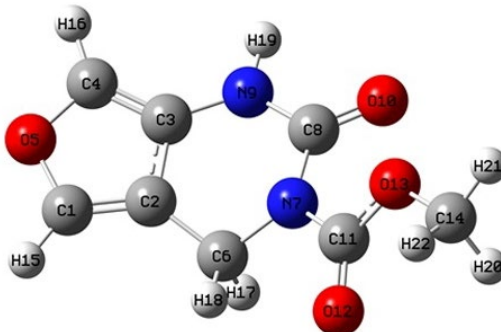


Fig. 1. Molecular configuration of FP.

The selected parameters for structural analysis, namely bond lengths, bond angles, and dihedral bond angles for the gas phase and in the DMSO solution of FP are given in Table 1. The Cartesian coordinates of the atoms in the minimized structure in the gas phase are given in supplementary S1. There are slight differences between the calculation in the gas phase and DMSO, except for dihedral angle H19-N9-C8-O10 as it turns to a positive value for the “in DMSO” case from its negative value for the gas phase. The dihedral angles (C6-C2-C3-N9) is $\sim 1(1)^\circ$ on average of the values obtained from both cases, while (C2-C6-N7-C8) is $\sim 44.58(35)^\circ$ exhibiting a bent pyrimidine ring. The flat dihedral angle (C1-C2-C3-N9) is $\sim 180^\circ$ showing that the (C6-C2-C3-N9) side of pyrimidine and furan rings are almost in the same plane while the angle $\sim 162.89(1,18)^\circ$ of (N9-C8-N7-C11) indicates the separation of the FP tail from (C2-C6-N7-C8) plane of the pyrimidine ring.

Table 1. Theoretical bond lengths (\AA), bond angles ($^\circ$), and dihedral bond angles ($^\circ$) of FP. Atom labels refer to Fig. 1.

Bond Length (\AA)			Bond Angles ($^\circ$)			Dihedral Bond Angles ($^\circ$)		
	Gas	DMSO		Gas	DMSO		Gas	DMSO
C1-C2	1.354	1.354	C1-C2-C3	105.97	106.06	H16-C4-O5-C1	-179.31	-179.55
C2-C3	1.423	1.423	C3-C4-O5	108.75	108.53	C1-C2-C3-C4	-0.16	-0.18
C1-H15	1.076	1.076	C3-C4-H16	134.58	134.48	C2-C3-C4-O5	-0.31	-0.27
C6-H18	1.086	1.085	H16-C4-O5	116.65	116.99	C4-C3-C2-C6	178.21	178.03
C14-H20	1.089	1.088	C4-O5-C1	107.53	107.68	C6-C2-C3-N9	-1.98	-2.19
C4-O5	1.371	1.373	O5-C1-C2	116.17	109.99	H19-N9-C8-O10	-1.34	0.23
C1-O5	1.364	1.364	N7-C11-O12	122.17	122.19	N9-C8-N7-C11	-164.08	-161.71
C8-O10	1.209	1.218	C11-O13-C14	115.19	115.61	N9-C8-N7-C6	28.54	29.15
C11-O12	1.210	1.215	C2-C6-N7	108.62	108.49	O10-C8-N7-C11	16.69	19.05
C14-O13	1.438	1.444	C6-N7-C8	120.75	120.65	C8-N7-C11-O12	-158.54	-158.83
C6-N7	1.484	1.488	N7-C8-N9	114.16	114.78	N7-C11-O13-C14	-178.25	-179.53
C8-N7	1.420	1.419	H19-N9-C3	121.91	121.24	C11-O13-C14-H21	177.59	178.19
C8-N9	1.382	1.370	N9-C8-O10	121.14	121.29	O12-C11-O13-C14	5.13	3.76
C3-N9	1.389	1.391	O10-C8-N7	124.69	123.92	C1-C2-C3-N9	179.63	179.60
C11-N7	1.399	1.395	C8-N7-C11	122.81	122.89	C2-C6-N7-C8	-44.95	-44.22
N9-H19	1.009	1.009	O12-C11-O13	124.75	124.35	C6-C2-C3-N9	-1.99	-2.19

The charge distribution in the atoms in the molecule is important for determining the electrostatic interaction and molecular force fields [53,54]. The atomic charge distributions of the FP are obtained by Mulliken Population Analysis (MPA), and Natural Population Analysis (NPA) methods within the framework Gaussian 09, which are listed in Table 2. There are differences when comparing the calculated atomic charges in the two methods. The charges such as C1, C2, and C3 are given discrepant by the two methods. MPA(C1) is -0.116 and NPA(C1) is 0.154 with a change in the sign. C2 has the same issue. Other atoms, even though they show the same sign, they differ in magnitude; for example, MPA(C3) is 0.312, and NPA(C3) is 0.078. However, the two methods provide good agreement on the charges of some atoms, such as O5, C4, C11, and H16. Overall, the oxygen and nitrogen atoms in the molecule are negatively charged, while the hydrogen atoms are positively charged, as usual. Amongst the carbon atoms, the highest negative charge is located on C14, while the highest positive charge is located on C11. The carbon atoms have negative or positive charges with respect to the electronegative atoms around them.

Table 2. Atomic charges of FP compound by Mulliken Population Analysis (MPA), and Natural Population Analysis (NPA) methods. Labels refer to Fig. 1.

Atom	MPA	NPA	Atom	MPA	NPA
C1	-0.116	0.154	O13	-0.318	-0.533
C2	0.549	-0.147	N7	-0.343	-0.564
C3	0.312	0.078	N9	-0.509	-0.616
C4	0.055	0.082	H15	0.181	0.200
C6	-0.963	-0.176	H16	0.180	0.200
C8	0.559	0.843	H17	0.161	0.205
C11	0.713	0.968	H18	0.212	0.244
C14	-0.121	-0.200	H19	0.275	0.412
O5	-0.366	-0.455	H20	0.164	0.186
O10	-0.458	-0.608	H21	0.145	0.187
O12	-0.468	-0.644	H22	0.157	0.184

The MPA and NPA methods obtain the results sensitively depending on their basis sets which induce change in the calculated net charges [54]. However, the results given by NPA are supposed to be more reliable as their calculations are based on the natural charges [55].

Molecular orbital energy analysis and electronic properties

Quantum chemical parameters were calculated with FMO analysis, and the highest occupied molecular orbital energy (E_{HOMO}), the lowest unoccupied molecular orbital energy (E_{LUMO}) together with the energy gap ($\Delta E = E_{\text{LUMO}} - E_{\text{HOMO}}$) given in Fig. 2. ΔE determines the molecular properties, namely softness and chemical reactivity [54,56-58]. In this respect, the ΔE energy difference of the FP calculated using the B3LYP and the 6-311++G (2d, p) basis set was 5.81 eV as a single molecule (5.64 eV in DMSO) related to the dipole moments of FP molecule which were found $\mu_{\text{gas}} = 1,92$ Debye and $\mu_{\text{DMSO}} = 2,99$ Debye in the gas phase and iMSO, respectively. The dipole moments were obtained by the conformal minimization of the molecule. These values make FP a high enough polarized pyrimidine molecule as compared to that of 4.86 eV for 5-Fluorouracil, a commercial anticancer reagent [59].

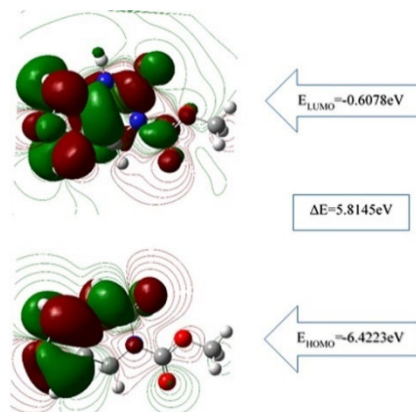


Fig. 2. E_{HOMO} and E_{LUMO} energy levels for FP.

The calculations of E_{HOMO} and E_{LUMO} energy levels lead to automatic determination of ionization energy (I) and electron affinity (A) which are expressed as

$$I = -E_{\text{HOMO}} \quad (1)$$

and

$$A = -E_{\text{LUMO}} \quad (2)$$

As E_{HOMO} indicates the electron-donating ability while E_{LUMO} refers to the electron-accepting ability. Once reaching the concerning parameters above, some characterizing parameters such as electronegativity (χ), chemical hardness (η), and softness (σ) from the following relations:

$$\chi = \frac{I + A}{2} \quad (3)$$

$$\eta = \frac{I - A}{2} \quad (4)$$

and

$$\sigma = \frac{1}{\eta} \quad (5)$$

The molecular electronic properties of FP obtained are given in Table 3. The high electronegativity values $\chi_{\text{gas}} = 3.51 \text{ eV}$ and $\chi_{\text{DMSO}} = 3.53 \text{ eV}$ indicates the strong attraction to covalent bonds [34]. Also, the large chemical hardness $\eta_{\text{gas}} = 2.91 \text{ eV}$ and $\eta_{\text{DMSO}} = 2.82 \text{ eV}$ indicates chemical stability, and the molecule can be considered as nontoxic because of the low softness values $\sigma_{\text{gas}} = 0.34 \text{ eV}^{-1}$ and $\sigma_{\text{DMSO}} = 0.35 \text{ eV}^{-1}$.

Table 3. Electronic structure values of FP.

Phase	$E_{\text{HOMO}}(\text{eV})$	$E_{\text{LUMO}}(\text{eV})$	$\Delta E (\text{eV})$	$I(\text{eV})$	$A(\text{eV})$	$\chi(\text{eV})$	$\eta(\text{eV})$	$\sigma (\text{eV}^{-1})$
gas	-6.42	-0.61	5.81	6.42	0.61	3.51	2.91	0.34
DMSO	-6.36	-0.71	5.64	6.36	0.71	3.53	2.82	0.35

Molecular electrostatic potential

The molecular electrostatic potential of FP was calculated and shown in Fig. 3. It shows the positively charged parts of the molecule in blue colour and the negatively charged parts in red colour [60-62].

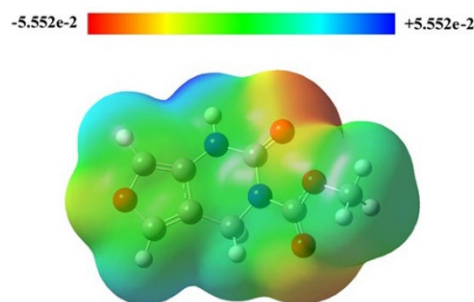


Fig. 3. Molecular electrostatic potential for FP.

As MEP allows us to have insight into the chemical reactivity of a molecule, the highest negative charge -0.059 region by red shade in Fig.3 is the electrophilic region. The negative electrostatic potential indicates the concentrated electron density in the molecule interacting with the receptors and forming hydrogen bonds with the positive sites of amino acids. They correspond to the tops of two carbonyls. The highest positive charge +0.059 region by blue shade is the nucleophilic region which corresponds to the hydrogen in the N-H bond. The green area can be considered almost a neutral region.

Experimental and theoretical ^{13}C NMR and ^1H NMR chemical shift values

Experimental and theoretical ^1H NMR and ^{13}C NMR chemical shift values of FP are listed in Table 4 according to TMS δ/ppm . The experimental NMR values were taken in DMSO [19], and theoretical NMR data were calculated in the gas phase and DMSO phase. In the FP structure, there are five different hydrogens attached to aliphatic and aromatic carbons and amine-bound, and all H peaks were observed as a singlet. In addition, eight different carbon peaks were found in the aliphatic, aromatic, and carbonyl structures.

When discussing the ^1H NMR spectra of the FP, the experimental chemical shift values of the protons-bounded aliphatic carbons were observed as a singlet in a value, while the theoretical chemical shift values were seen as two different peaks. The experimental value of the ring protons, CH_2 was at 4.71 ppm as a singlet, while the theoretical values of H17 and H18 were 4.50 and 5.19 ppm, respectively. Ester protons, CH_3 experimental value was in the 3.78 ppm as a singlet, while the theoretical values of H21 and H20, H22 were in 3.72 and 3.87 ppm, respectively. The experimental value of amine proton was 9.96 ppm as a broad singlet, whereas the theoretical value of H19 was 6.42 ppm. The experimental values of aromatic ring protons were at 7.27 and 7.46 ppm, whereas the theoretical values of H15 and H16 were at 7.31 and 7.37 ppm, respectively.

Table 4. The experimental and theoretical ^1H NMR and ^{13}C NMR chemical shift values of FP according to TMS δ/ppm . (s.: singlet, br.: broad Assign.: assignments) The hydrogen and carbon labels can be followed in Fig. 1.

^1H NMR				
Experimental		Theoretical		
Assign.	$\delta(\text{ppm})$	Assign.	Gas phase	DMSO
CH_3	3.73 (s)	H21	3.56	3.72
		H20, H22	3.83	3.87
CH_2	4.71 (s)	H17	4.34	4.50
		H18	5.14	5.19
NH	9.96 (br. s)	H19	5.75	6.42
CH (arom.)	7.27 (s)	H15	7.05	7.31
CH (arom.)	7.46 (s)	H16	7.12	7.37

¹³ C NMR				
Experimental		Theoretical		
Assign.	δ (ppm)	Assign.	Gas phase	DMSO
CH ₂	29.74	C6	43.24	44.06
CH ₃	54.28	C14	54.87	55.95
C(arom.)	111.13	C2	117.37	117.28
CH(arom.)	124.88	C4	126.54	129.19
C(arom.)	126.17	C3	132.70	131.85
CH(arom.)	136.96	C1	140.50	141.87
C=O	150.05	C8	153.01	156.06
C=O	155.32	C11	162.07	163.40

Considering the ¹³C NMR spectra of the FP, the experimental values of the aliphatic ring (CH₂) and ester methyl carbon peaks (CH₃) were at 29.74 and 54.28 ppm, whereas the theoretical values of C6 and C14 were at 44.06 and 55.95 ppm, respectively. The aromatic carbons' experimental values were 111.13, 124.88, 126.17, and 136.96 ppm, whereas theoretical values of C2, C4, C3, and C1 were 117.28, 129.18, 131.85, and 141.87, respectively. The experimental values of ring carbonyl carbon and aliphatic carbonyl carbon were at 150.05 and 155.32 ppm, while theoretical values of C8 and C11 were at 156.06 and 163.40 ppm, respectively. According to the NMR results, the experimental and theoretical chemical shift values are compatible. The theoretical and experimental NMR spectra were given in the supplementary (S2-S5).

Experimental and theoretical vibration frequencies

The molecular structure of FP contains twenty-two atoms, which gives forty-four normal modes of vibrations. While experimental vibration values were taken from the literature [19], theoretical vibration values were calculated using the DFT/B3LYP method and 6-311++G (2d, p) basis set. The FTIR spectrum was analyzed based on characteristic peaks such as amine, aromatic, carbonyl, and CH₂ vibrations. The experimental and theoretical values of the vibrational wavenumber of FP are shown in Fig. 4. For analysis, all the calculated FTIR, compared to experimental values, and details of the percentage of potential energy distribution (PED) assignment are listed in Table 5. When performing PED assignments, it was found that there were thirty-four stretching vibrations, thirty-six in-plane bending vibrations, four out of plane bending vibrations, and eighteen torsional vibrations. When the experimental and theoretical values were compared, they were found to be well-matched.

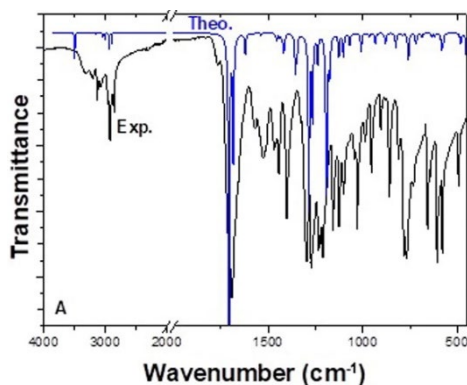


Fig. 4. Experimental and theoretical FTIR spectrum of FP (cm^{-1}).

Table 5. Experimental and theoretical FTIR values of FP (cm^{-1}).

No	Experimental	Theoretical		Vibration assignment (PED)
		Unscaled	Scaled	
1	3321	3633	3492	vN9-H19 (100)
2	3071	3282	3155	vC4-H16 (95)
3	3048	3271	3144	vC1-H15 (95)
4		3158	3036	vC14-H21 (80), vC14-H20 (19), vC14-H22 (19)
5		3137	3016	vC6-H18 (98)
6	2980	3127	3006	vC14-H20, vC14-H22 (100)
7		3054	2936	vC14-H20, vC14-H21 (80)
8	2925	3010	2894	vC6-H17 (98)
9	1694	1777	1708	vC8-O10 (77)
10	1686	1752	1684	vC11-O12 (81)
11	1571	1686	1621	vC1-C2, vC3-C4 (76)
12	1528	1599	1537	vC1-C2 (52), vC3-N9 (52) δ H15-C1-O5 (12), δ H16-C4-O5 (12), δ C1-O5-C4 (11), δ C3-C4-O5 (11)
13	1465	1513	1454	δ H18-C6-H17 (74), τ H18-C6-C2-C1 (12)
14	1458	1497	1439	δ H20-C14-H22 (70), τ H20-C14-O13-C11 (21), τ H22-C14-O13-C11-(21)
15	1440	1485	1428	δ H21-C14-H20 (38), δ H22-C14-H21 (35), τ H21-C14-O13-C11 (15), τ H20-C14-O13-C11 (10), τ H22-C14-O13-C11 (10)
16	1406	1469	1412	δ H19-N9-C3, δ C2-C1-O5 (44)
17	1326	1411	1356	δ C6-N7-C8 (14)
18	1301	1402	1348	vC3-C4, vC3-N9 (24)
19	1293	1337	1285	vC11-N7 (44), vC11-O13 (44), δ H17-C6-C2 (10)
20	1270	1289	1239	vC8-N9 (10)
21	1234	1244	1196	δ H16-C4-O5, δ H15-C1-O5 (67)
22	1205	1224	1177	δ C8-N7-C11, δ N9-C8-O10, δ C3-N9-C8, δ O12-C11-O13, δ C3-C4-O5 (15)
23	1159	1172	1127	vC1-O5, vC6-N7 (54)

24	1128	1147	1103	vC1-O5, vC4-O5, vC6-N7 (61)
25	1100	1112	1069	vC11-N7 (22), vC11-O13 (22), vC14-O13 (11)
26	1040	1049	1008	vC1-O5, vC4-O5 (64)
27	985	1005	966	τ H17-C6-C2-C1 (26)
28	951	916	881	δ C1-O5-C4, δ N7-C8-N9 (44)
29	902	858	825	δ C3-C4-O5, δ N9-C8-O10, δ N7-C8-N9 (76)
30	859	822	790	δ O12-C11-O13, δ C11-O13-C14, δ C3-N9-C8 (41)
31	781	790	759	τ H15-C1-O5-C4 (57), τ C1-O5-C4-C3 (11), γ O12-N7-O13-C11 (66)
32	766	749	720	γ O10-N9-N7-C8 (85)
33	724	743	714	vC8-N7 (12), τ C6-N7-C8-N9 (10)
34	660	715	687	τ H16-C4-O5-C1 (45), τ C2-C1-O5-C4 (18), τ C1-O5-C4-C3 (18)
35	608	606	583	δ C3-N9-C8, δ O12-C11-O13, δ N9-C8-O10 (35)
36	580	502	483	τ H19-N9-C3-C2 (30)
37	489	435	418	δ N7-C11-O13, δ N9-C8-O10, - δ O12-C11-O13, δ C8-N7-C11 (49)
38		334	321	γ N9-C2-C4-C3 (23)
39		324	311	δ C11-O13-C14, δ C8-N7-C11 (60)
40		296	285	τ N7-C8-N9-C3 (10)
41		257	247	δ C8-N7-C11, δ C11-O13-C14, δ N7-C11-O13, δ N7-C8-N9 (10)
42		222	213	τ C8-N9-C3-C2 (34), τ C14-O13-C11-N7 (11)
43		169	162	γ C11-C6-C8-N7 (17)
44		62	60	τ O13-C11-N7-C6 (71)

NH vibrations

The stretching vibrations of the amide NH bond were observed around 3300-3600 cm⁻¹ [62,63]. In FP, N9-H19 stretching vibration was theoretically observed at 3492 cm⁻¹ with PED contribution is 100 % and experimentally at 3321 cm⁻¹ as a strong peak. Furthermore, H19-N9-C3 in-plane bending vibration was observed theoretically at 1412 cm⁻¹ and experimentally at 1406 cm⁻¹. The H19-N9-C3-C2 torsional vibration was observed theoretically at 483 cm⁻¹ and experimentally at 580 cm⁻¹.

Aromatic CH vibrations

Aromatic CH bond stretching vibrations are usually just over 3000 cm⁻¹ [63,64]. There are two different aromatic CH in the FP structure, and their vibrational values were very close. C4-H16 and C1-H15

stretching vibrations were theoretically observed at 3144 cm^{-1} and 3157 cm^{-1} , and experimentally at 3193 cm^{-1} and 3139 cm^{-1} , respectively. H16-C4-O5 and H15-C1-O5 in-plane bending vibrations had the same value and two vibrations; theoretically observed at 1537 cm^{-1} and 1196 cm^{-1} , experimentally at 1528 cm^{-1} and 1234 cm^{-1} . Moreover, H15-C1-O5-C4 and H16-C4-O5-C1 torsional vibrations were observed theoretically at 759 cm^{-1} and 687 cm^{-1} experimentally at 781 cm^{-1} and 660 cm^{-1} , respectively.

Carbonyl vibrations

Depending on the electronegative atoms attached to the carbonyl group, the carbonyl group gives a stretching vibration in the range of $1650\text{-}1800\text{ cm}^{-1}$ [62,63]. There are two different carbonyl groups located between nitrogen-nitrogen and oxygen-nitrogen in the FP structure. The carbonyl group (C8-O10) located between nitrogen and nitrogen in the ring structure gave a higher frequency peak than the other (C11-O12). While C8-O10 and C11-O12 stretching frequency were observed theoretically at 1708 and 1684 cm^{-1} , experimentally at 1694 and 1686 cm^{-1} , respectively. In addition, N9-C8-O10 in-plane bending vibrations were theoretically observed at 1177 , 825 , 583 , 418 cm^{-1} , and experimentally at 1205 , 902 , 608 , 489 cm^{-1} .

CH_2 vibrations

The characteristic vibration of the CH_2 is the stretching vibration in the range of $2900\text{-}3000\text{ cm}^{-1}$ and the in-plane bending vibration around 1450 cm^{-1} [65]. The C6-H18 and C6-H17 stretching vibrations were observed theoretically at 3016 and 2894 cm^{-1} , respectively, and experimentally at 2925 cm^{-1} . H18-C6-H17 in-plane bending vibration was observed theoretically at 1454 cm^{-1} and experimentally at 1465 cm^{-1} .

Molecular docking

Molecular docking calculations are used to gain information about ligand-receptor interactions and play an important role in drug discovery. As a result of these calculations, it can be found out which region of the protein the ligand binds to, what kind of interactions it makes, and their binding energies [54,60,66,67]. In this study, molecular docking calculations with the brain (PDB ID: 1QHT), breast (PDB ID: 1JNX), gastric (PDB ID: 1BJ7), liver (PDB ID: 3WZE), lung (PDB ID: 2ITO), and skin (PDB ID: 2VCJ) cancer proteins to see the biological potential of FP were examined. Many docking studies were carried out and the lowest energies interaction was selected. The calculated lowest binding energies of the target biomolecules and FP are given in Table 6. In addition, FP makes more stable interactions with brain and liver cancer cells than others. The binding sites of FP with target biomolecules are shown in Figure 5. Looking at the structure of the FP compound, it is seen that it is an active compound-containing pyrimidine ring, furan ring, and ester. When calculated results are examined, FP makes hydrophobic interactions with ARG130, ARG132, TRP228, ARG236, ILE238, MET240, ARG292 amino acids in brain cancer protein, SER1755, ARG1758, LYS1759, ILE1760, ARG1762, TYR1845, GLN1846, CYS1847 amino acids in breast cancer protein, ARG40, ILE149, ASP152, ASN153, CYS154, PRO156 amino acids in gastric cancer protein, HIS816, LYS868, ALA881, SER884, GLU885, ILE888, ARG1027, ASP1046, GLY1048, LEU1049, BAX1201 amino acids in liver cancer protein, SER 719, ALA722, PHE723, VAL726, LYS745, ARG841, LEU844, ASP855, IRE2020 amino acids in lung cancer protein, ARG46, GLU47, SER50, ASN51, GLY132, GLN133, GLY135, GLY137 amino acids in skin cancer protein.

Table 6. The binding energies of FP and target biomolecules.

Protein (PDB ID)	Types of cancer	Binding energy (kcal/mol)
1QH4	Brain cancer	-6.1
1JNX	Breast cancer	-4.9
1BJ7	Gastric cancer	-4.4
3WZE	Liver cancer	-6.1
2ITO	Lung cancer	-5.9
2VCJ	Skin cancer	-4.8

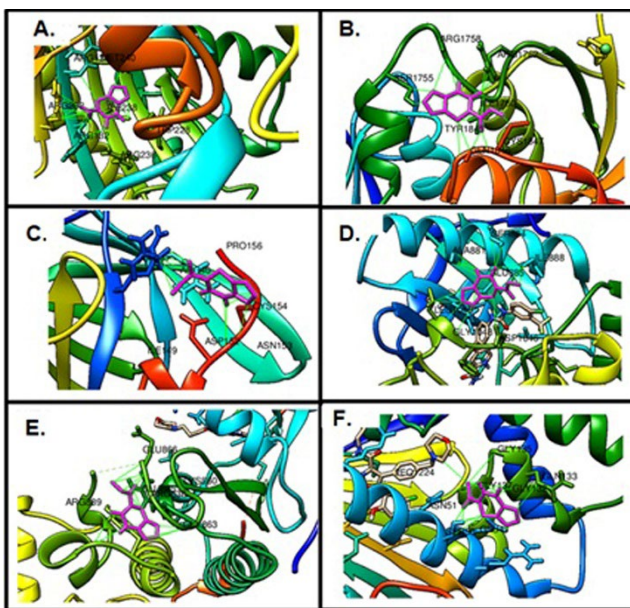


Fig. 5. The binding site of FP on target proteins, (A) Brain cancer protein, (B) Breast cancer protein, (C) Gastric cancer protein, (D) Liver cancer protein, (E) Lung cancer protein, (F) Skin cancer protein.

H bonds are strong interactions that hold molecules together and the number of the H bonds gives information about the strength of the interaction. The H bond interactions between FP and targeted biomolecules are given in Fig. 6. Also, the number of H bonds made by FP with each biomolecule and the atoms forming the H bond are listed in Table 7.

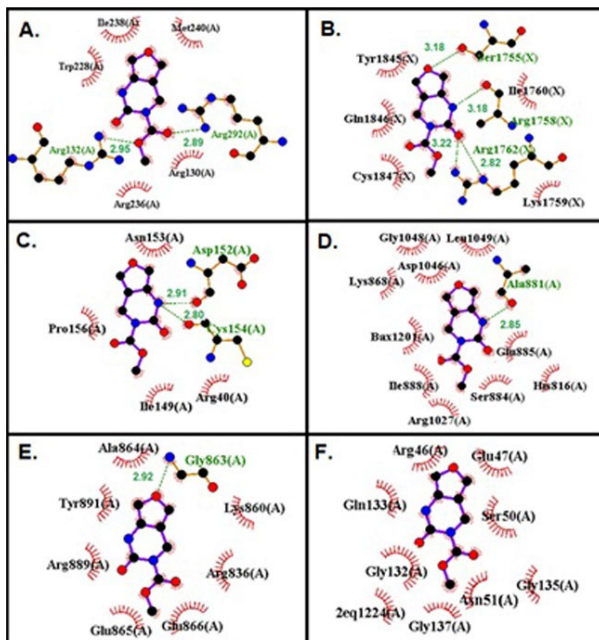


Fig. 6. The H bond interactions between FP and target proteins, (A) Brain cancer protein, (B) Breast cancer protein, (C) Gastric cancer protein, (D) Liver cancer protein, (E) Lung cancer protein, (F) Skin cancer protein.

Table 7. Summary of hydrogen bonding of fuopyrimidine molecule with different types of biomolecule targets.

Protein (PDB ID)	Number of H bond	Bonded residues		Bond distance (Å)
1QH4	2	Protein ARG292:HN	Ligand: O12	2.89
		Protein ARG132:HN	Ligand:O13	2.95
1JNX	4	Protein SER1755:OH	Ligand: O5	3.18
		Protein ARG1758:O	Ligand: N9H19	3.18
		Protein ARG1762:HN	Ligand: O12	2.82
		Protein ARG1762:HN	Ligand: O12	3.22
1BJ7	2	Protein ASP152:O	Ligand: N9H19	2.91
		Protein CYS154:O	Ligand: N9H19	2.80
3WZE	1	Protein ALA881:O	Ligand: N9H19	2.85
2ITO	1	Protein LYS745:NH	Ligand: O12	3.21
2VCJ	-	-	-	-

When it is examined in this study, FP makes two H bonds with ARG 132, ARG 292 amino acids in brain cancer protein, it makes four H bonds with SER1755, ARG1758, ARG1752 amino acids in breast cancer protein, it makes two H bonds with ASP152, CYS 154 amino acids in gastric cancer protein, it makes one H bond with ALA881 amino acid liver cancer protein, it makes one H bond with GLY863 amino acid in liver cancer protein, it doesn't make H bond with an amino acid in skin cancer protein, and it makes two H bond with DA5.

When the H bonds were examined, it was seen that N9 in the FP structure is the H bond donor, and O5, O12, and O13 are H bond acceptors. It can be said that N9 and O12 atoms in the FP structure are the most active ones in forming H bonds.

Evaluation of pharmacokinetics and drug-likeness properties of FP

By evaluating the pharmacokinetic properties, toxicity, and bioavailability of the compounds, their usage or development as a drug can be achieved [68-70]. As shown in Table 8, FP follows the Lipinski Rule, Pfizer Rule, and GlaxoSmithKline Rule as a drug candidate. According to the ADME result, FP has a high GI (gastrointestinal) absorption value, which means that the drug is rapidly absorbed.

The molecular weight of FP being 196.16 g/mol and having 2 rotatable bonds indicate the conformity of the molecule. The number of hydrogen bond acceptors and donors is within the expected range, which indicates that they can interact strongly enough. Log P is a measure of the hydrophilicity and hydrophobicity of a molecule. The log P value of FP is compatible with the Lipinski rule. The topological polar surface area (TPSA) value of FP 71.78 Å² indicates that they have good permeability during the cellular plasma membrane and blood-brain barrier.

Table 8. Data of Lipinski rule, Pharmacokinetics, and Drug likeness.

Mw	NBR	HBA	HBD	TPSA/A2 (≤140)	Consensus Log Po/w	Bioavailability Score	GI abs.
196,16	2	4	1	71.78	0.21	0.55	high

Mw: Molecular weight, NBR: Number of rotatable bonds, HBA: Number of Hydrogen bond acceptors, HBD: Number of Hydrogen bond donors, TPSA: Topological polar surface area, Consensus Log Po/w: Log Poctane/water, GI: Gastrointestinal.

The ADMET data of the FP which is computationally forecasted from its given molecular structure are shown in Table 9. It is exhibited that the FP has oral bioavailability, and is rapidly absorbed in the human intestine. Also, FP does not show skin sensitivities, AMES toxicity, and respiratory toxicity. The FP is not a P-glycoprotein inhibitor or substrate. Since P-glycoprotein pumps drugs back into the lumen, reducing drug absorption, it can be said that the bioavailability and bioactivity of the FP are high. A summary of the ADMET properties of FP is shown in Fig. 7.

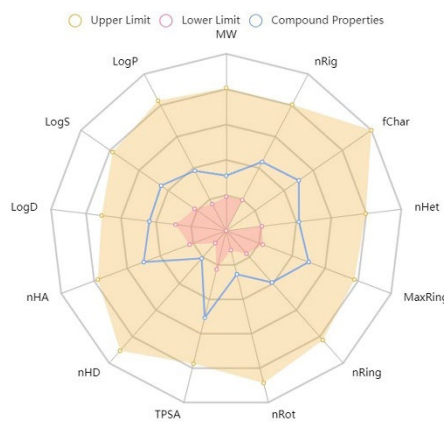


Fig. 7. Radar chart involved in ADMET properties of FP.

Table 9. Pharmacokinetics and ADMET Data.

Lipinski Rule	yes	Respiratory toxicity	no
Pfizer Rule	yes	P-glycoprotein inhibitor	no
GlaxoSmithKline Rule	yes	P-glycoprotein substrate	no
Human Intestinal Absorption	high	Solubility	yes
AMES toxicity	no	hERG (the human Ether-à-go-go-Related Gene) inhibitor	no
Skin sensitization	no		

Conclusions

In this study, the FP geometry was optimized using the B3LYP/6-311G++ (2d, p) method within density functional theory. The bond lengths, bond angles, dihedral angles, MEP, dipole moments, HOMO, and LUMO of FP were obtained with the Gaussian G09w program. Theoretical FTIR and NMR spectrum values were found to be compatible with the experimental spectrum values. Due to the wide biological activities of pyrimidine compounds, molecular docking studies of FP were carried out with various biomolecules. As a result of molecular docking studies, it was determined that N9 and O12 atoms of FP were the most active ones, and they make hydrogen bonds and hydrophobic interactions with biomolecules. Data on the pharmacokinetic and drug-likeness of FP was observed. For future studies, the synthesis of new dihydrafuro [3,4-d] pyrimidine derivatives may be desirable and could be a source of similar studies to determine their mechanisms as potential anticancer agents.

References

1. Abdel-Aziz, S. A.; Taher, E. S.; Lan, P.; Asaad, G. F.; Gomaa, H. A.; El-Koussi, N. A.; Youssif, B. G. *Bioorg. Chem.* **2021**, *111*, 104890. DOI: <https://doi.org/10.1016/j.bioorg.2021.104890>.
2. Aksinenko, A. Y.; Goreva, T. V.; Epishina, T. A.; Trepalin, S. V.; Sokolov, V. B. *J. Fluor. Chem.* **2016**, *188*, 191-195. DOI: <https://doi.org/10.1016/j.jfluchem.2016.06.019>.
3. Ballesteros-Casallas, A.; Paulino, M.; Vidossich, P.; Melo, C.; Jiménez, E.; Castillo, J.-C.; Portilla, J.; Miscione, G. P. *Eur. J. Med. Chem.* **2022**, *4*, 100028. DOI: <https://doi.org/10.1016/j.ejmer.2021.100028>.
4. Basyouni, W. M.; Abbas, S. Y.; El-Bayouki, K. A.; Dawood, R. M.; El Awady, M. K.; Abdelhafez, T. H. *J. Heterocycl. Chem.* **2021**, *58*, 1766-1774. DOI: <https://doi.org/10.1002/jhet.4307>.
5. Elkanzi, N. A. A. *Orient. J. Chem.* **2020**, *36*, 1001-1015. DOI: <http://dx.doi.org/10.13005/ojc/360602>.
6. Ali, F.; Khan, K. M.; Salar, U.; Iqbal, S.; Taha, M.; Ismail, N. H.; Perveen, S.; Wadood, A.; Ghufran, M.; Ali, B. *Bioorg. Med. Chem.* **2016**, *24*, 3624-3635. DOI: <https://doi.org/10.1016/j.bmc.2016.06.002>.
7. Katariya, K. D.; Reddy, D. V. *J. Mol. Struct.* **2022**, *1253*, 132240. DOI: <https://doi.org/10.1016/j.molstruc.2021.132240>.
8. Lamie, P. F.; Philoppes, J. N. *Bioorg. Chem.* **2021**, *116*, 105335. DOI: <https://doi.org/10.1016/j.bioorg.2021.105335>.
9. Manzoor, S.; Prajapati, S. K.; Majumdar, S.; Raza, M. K.; Gabr, M. T.; Kumar, S.; Pal, K.; Rashid, H.; Kumar, S.; Krishnamurthy, S. *Eur. J. Med. Chem.* **2021**, *215*, 113224. DOI: <https://doi.org/10.1016/j.ejmech.2021.113224>.
10. Raju, K. S.; AnkiReddy, S.; Sabitha, G.; Krishna, V. S.; Sriram, D.; Reddy, K. B.; Sagurthi, S. R. *Bioorg. Med. Chem. Lett.* **2019**, *29*, 284-290. DOI: <https://doi.org/10.1016/j.bmcl.2018.11.036>.
11. Fei, X.; Wang, J.-Q.; Miller, K. D.; Sledge, G. W.; Hutchins, G. D.; Zheng, Q.-H. *Nucl. Med. Biol.* **2004**, *31*, 1033-1041. DOI: <https://doi.org/10.1016/j.nucmedbio.2004.02.006>.
12. Scappini, B.; Gianfaldoni, G.; Caracciolo, F.; Mannelli, F.; Biagiotti, C.; Romani, C.; Pogliani, E. M.; Simonetti, F.; Borin, L.; Fanci, R. *Am. J. Hematol.* **2012**, *87*, 1047-1051. DOI: <https://doi.org/10.1002/ajh.23308>.
13. Halbrook, C. J.; Pontious, C.; Kovalenko, I.; Lapienyte, L.; Dreyer, S.; Lee, H.-J.; Thurston, G.; Zhang, Y.; Lazarus, J.; Sajjakulnukit, P. *Cell Metab.* **2019**, *29*, 1390-1399. e6. DOI: <https://doi.org/10.1016/j.cmet.2019.02.001>.
14. Verissimo, L. M.; Cabral, I.; Cabral, A. M.; Utzeri, G.; Veiga, F. J.; Valente, A. J.; Ribeiro, A. C. *J. Chem. Thermodyn.* **2021**, *161*, 106533. DOI: <https://doi.org/10.1016/j.jct.2021.106533>.
15. Abd El-Mageed, M. M.; Eissa, A. A.; Farag, A. E.-S.; Osman, E. E. A. *Bioorg. Chem.* **2021**, *116*, 105336. DOI: <https://doi.org/10.1016/j.bioorg.2021.105336>.
16. Gregorić, T.; Sedić, M.; Grbčić, P.; Paravić, A. T.; Pavelić, S. K.; Cetina, M.; Vianello, R.; Raić-Malić, S. *Eur. J. Med. Chem.* **2017**, *125*, 1247-1267. DOI: <https://doi.org/10.1016/j.ejmech.2016.11.028>.
17. Hossam, M.; Lasheen, D. S.; Ismail, N. S.; Esmat, A.; Mansour, A. M.; Singab, A. N. B.; Abouzid, K. A. *Eur. J. Med. Chem.* **2018**, *144*, 330-348. DOI: <https://doi.org/10.1016/j.ejmech.2017.12.022>.
18. Frisch, M. J.; Trucks, G. W.; Schlegel, H. B.; Scuseria, G. E.; Robb, M. A.; Cheeseman, J. R.; Scalmani, G.; Barone, V.; Mennucci, B.; Petersson, G. A.; Nakatsuji, H.; Caricato, M.; Li, X.; Hratchian, H. P.; Izmaylov, A. F.; Bloino, J.; Zheng, G.; Sonnenberg, J. L.; Hada, M.; Ehara, M.; Toyota, K.; Fukuda, R.; Hasegawa, J.; Ishida, M.; Nakajima, T.; Honda, Y.; Kitao, O.; Nakai, H.; Vreven, T.; Montgomery, J. A.; Peralta, J. E.; Ogliaro, F.; Bearpark, M.; Heyd, J. J.; Brothers, E.; Kudin, K. N.; Staroverov, V. N.; Kobayashi, R.; Normand, J.; Raghavachari, K.; Rendell, A.; Burant, J. C.; Iyengar, S. S.; Tomasi, J.; Cossi, M.; Rega, N.; Millam, J. M.; Klene, M.; Knox, J. E.; Cross, J. B.; Bakken, V.; Adamo, C.; Jaramillo, J.; Gomperts, R.; Stratmann, R. E.; Yazyev, O.; Austin, A. J.; Cammi, R.; Pomelli, C.; Ochterski, J. W.; Martin, R. L.; Morokuma, K.; Zakrzewski, V. G.; Voth, G.

- A.; Salvador, P.; Dannenberg, J. J.; Dapprich, S.; Daniels, A. D.; Farkas; Foresman, J. B.; Ortiz, J. V.; Cioslowski, J.; Fox, D. J., Gaussian 09, Revision B.01, Gaussian Inc., Wallingford CT, **2009**.
19. Yilmaz, A. S.; Kaçan, M. *Tetrahedron*. **2017**, *73*, 4509-4512. DOI: <https://doi.org/10.1016/j.tet.2017.05.072>.
20. Daina, A.; Michielin, O.; Zoete, V. *Sci Rep.* **2017**, *7*, 42717. DOI: <https://doi.org/10.1038/srep42717>.
21. Yang, H.; Lou, C.; Sun, L.; Li, J.; Cai, Y.; Wang, Z.; Li, W.; Liu, G.; Tang, Y. *Bioinformatics*. **2018**, *35*, 1067-1069. DOI: <https://doi.org/10.1093/bioinformatics/bty707>.
22. Qu, R.; Zhang, X.; Zhang, Q.; Yang, X.; Wang, Z.; Wang, L. *Spectrochim. Acta A Mol. Biomol. Spectrosc.* **2011**, *81*, 261-269. DOI: <https://doi.org/10.1016/j.saa.2011.06.008>.
23. Manikandan, D.; Swaminathan, J.; Tagore, S. S.; Gomathi, S.; Sabarinathan, N.; Ramalingam, M.; Balasubramani, K.; Sethuraman, V. *Spectrochim. Acta A Mol. Biomol. Spectrosc.* **2020**, *239*, 118484. DOI: <https://doi.org/10.1016/j.saa.2020.118484>.
24. Foresman, J.; Frish, E. in: *Exploring Chemistry with Electronic Structure Methods*, Gaussian Inc., Pittsburgh, USA, **1996**.
25. Sayin, K.; Karakaş, D. *Spectrochim. Acta A Mol. Biomol. Spectrosc.* **2015**, *144*, 176-182. DOI: <https://doi.org/10.1016/j.saa.2015.02.086>.
26. Uluçam, G.; Okan, S. E.; Aktaş, Ş.; Yentürk, B. *J. Mol. Struct.* **2021**, *1230*, 129941. DOI: <https://doi.org/10.1016/j.molstruc.2021.129941>.
27. Dennington, R.; Keith, T.; Millam, J. Gauss View, Version 5. Semichem Inc., Shawnee Mission, **2009**.
28. Zhen, Y.; Shan, X.; Li, Y.; Lin, Z.; Zhang, L.; Lai, C.; Qin, F. *Phytomed. Plus.* **2022**, 100244. DOI: <https://doi.org/10.1016/j.phyplu.2022.100244>.
29. Yadav, V.; Krishnan, A.; Baig, M. S.; Majeed, M.; Nayak, M.; Vohora, D. *Biophys. Chem.* **2022**, 285. DOI: <https://doi.org/10.1016/j.bpc.2022.106808>.
30. Anju, K.; Shoba, G.; Sumita, A.; Balakumaran, M. D.; Vasanthi, R.; Kumaran, R. *Spectrochim. Acta, Part A*. **2021**, *258*, 119814. DOI: <https://doi.org/10.1016/j.saa.2021.119814>.
31. Crampon, K.; Giorkallos, A.; Deldossi, M.; Baud, S.; Steffenel, L. A. *Drug Discovery Today*. **2021**, 151-164. DOI: <https://doi.org/10.1016/j.drudis.2021.09.007>.
32. Trott, O.; Olson, A. J. *J. Comput. Chem.* **2010**, *31*, 455-461. DOI: <https://doi.org/10.1002/jcc.21334>.
33. Morris, G. M.; Huey, R.; Lindstrom, W.; Sanner, M. F.; Belew, R. K.; Goodsell, D. S.; Olson, A. J. *J. Comput. Chem.* **2009**, *30*, 2785-2791. DOI: <https://doi.org/10.1002/jcc.21256>.
34. Fatima, A.; Khanum, G.; Sharma, A.; Verma, I.; Arora, H.; Siddiqui, N.; Javed, S. *Polycycl. Aromat. Compd.* **2023**, *43*, 1263-1287. DOI: <https://doi.org/10.1080/10406638.2022.2026989>.
35. Yavuz, S. Ç.; Akkoç, S.; Tüzün, B.; Şahin, O.; Saripinar, E. *Synth. Commun.* **2021**, *51*, 2135-2159. DOI: <https://doi.org/10.1080/00397911.2021.1922920>.
36. Xavier, T.; Kenny, P. T.; Manimaran, D.; Joe, I. H. *Spectrochim. Acta A Mol. Biomol. Spectrosc.* **2015**, *145*, 523-530. DOI: <https://doi.org/10.1016/j.saa.2015.02.087>.
37. Suresh, D.; Amalanathan, M.; Joe, I. H.; Jothy, V. B.; Diao, Y.-P. *Spectrochim. Acta A Mol. Biomol. Spectrosc.* **2014**, *130*, 591-603. DOI: <https://doi.org/10.1016/j.saa.2014.03.043>.
38. Devi, K.S.; Subramani, P.; Parthiban, S.; Sundaraganesan, N. *J. Mol. Struct.* **2020**, *1203*, 127403. DOI: <https://doi.org/10.1016/j.molstruc.2019.127403>.
39. Adwin Jose, P.; Sankarganesh, M.; Dhaveethu Raja, J.; Senthilkumar, G. S.; Nandini Asha, R.; Raja, S. J.; Sheela, C. D. J. *Biomol. Struct. Dyn.* **2021**, *21*, 10715–10729. DOI: <https://doi.org/10.1080/07391102.2021.1947382>.
40. Rodriguez, A. C.; Park, H.-W.; Mao, C.; Beese, L. S. *J. Mol. Biol.* **2000**, *299*, 447-462. DOI: <https://doi.org/10.1006/jmbi.2000.3728>.
41. Williams, R. S.; Green, R.; Glover, J. *Nat. Struct. Biol.* **2001**, *8*, 838-842. DOI: <https://doi.org/10.1038/nsb1001-838>.
42. Rouvinen, J.; Rautiainen, J.; Virtanen, T.; Zeiler, T.; Kauppinen, J.; Taivainen, A.; Mäntylä, R. *J. Biol. Chem.* **1999**, *274*, 2337-2343. DOI: <https://doi.org/10.1074/jbc.274.4.2337>.

43. Okamoto, K.; Ikemori-Kawada, M.; Jestel, A.; von König, K.; Funahashi, Y.; Matsushima, T.; Tsuruoka, A.; Inoue, A.; Matsui, J. *ACS Med. Chem. Lett.* **2015**, *6*, 89-94. DOI: <https://doi.org/10.1021/ml500394m>.
44. Yun, C.-H.; Boggon, T. J.; Li, Y.; Woo, M. S.; Greulich, H.; Meyerson, M.; Eck, M. J. *Cancer cell.* **2007**, *11*, 217-227. DOI: <https://doi.org/10.1016/j.ccr.2006.12.017>.
45. Brough, P. A.; Aherne, W.; Barril, X.; Borgognoni, J.; Boxall, K.; Cansfield, J. E.; Cheung, K.-M. J.; Collins, I.; Davies, N. G.; Drysdale, M. J. *J. Med. Chem.* **2008**, *51*, 196-218. DOI: <https://doi.org/10.1021/jm701018h>.
46. Masand, V. H.; Rastija, V. *Chemom. Intell. Lab. Syst.* **2017**, *169*, 12-18. DOI: <https://doi.org/10.1016/j.chemolab.2017.08.003>.
47. DeLano, W. L. <http://www.pymol.org>, 2002.
48. Pettersen, E. F.; Goddard, T. D.; Huang, C. C.; Couch, G. S.; Greenblatt, D. M.; Meng, E. C.; Ferrin, T. E. *J. Comput. Chem.* **2004**, *25*, 1605-1612. DOI: <https://doi.org/10.1002/jcc.20084>.
49. Laskowski, R. A.; Swindells, M. B. *J. Chem. Inf. Model.* **2011**, *51*, 2778-2786 DOI: <https://doi.org/10.1021/ci200227u>.
50. Lipinski, C. A. *Drug. Discov. Today. Technol.* **2004**, *1*, 337-41. DOI: <https://doi.org/10.1016/j.ddtec.2004.11.007>.
51. Cheng, F.; Li, W.; Zhou, Y.; Shen, J.; Wu, Z.; Liu, G.; Lee, P. W.; Tang, Y. *J. Chem. Inf. Model.* **2012**, *52*, 3099-3105. DOI: <https://doi.org/10.1021/ci300367a>.
52. Saravanan, R.; Seshadri, S.; Gunasekaran, S.; Mendoza-Meroño, R.; García-Granda, S. *Spectrochim. Acta A Mol. Biomol. Spectrosc.* **2015**, *139*, 321-328. DOI: <https://doi.org/10.1016/j.saa.2014.12.026>.
53. Demircioğlu, Z.; Kaştaş, Ç. A.; Büyükgüngör, O. **2015**, *1091*, 183-195. DOI: <https://doi.org/10.1016/j.molstruc.2015.02.076>.
54. Obu, Q. S.; Louis, H.; Odey, J. O.; Eko, I. J.; Abdullahe, S.; Ntui, T. N.; Offiong, O. E. *J. Mol. Struct.* **2021**, *1244*, 130880. DOI: <https://doi.org/10.1016/j.molstruc.2021.130880>.
55. Mumit, M. A.; Pal, T. K.; Alam, M. A.; Islam, M. A.-A.-A.; Paul, S.; Sheikh, M. C. *J. Mol. Struct.* **2020**, *1220*, 128715. DOI: <https://doi.org/10.1016/j.molstruc.2020.128715>.
56. Ouaket, A.; Chraka, A.; Raissouni, I.; El Amrani, M. A.; Berrada, M.; Knouzi, N. *J. Mol. Struct.* **2022**, *1259*, 132729. DOI: <https://doi.org/10.1016/j.molstruc.2022.132729>.
57. Abdou, A.; Omran, O. A.; Nafady, A.; Antipin, I. S. *Arabian J. Chem.* **2022**, *15*, 103656. DOI: <https://doi.org/10.1016/j.arabjc.2021.103656>.
58. Ulucam, G.; Yenturk, B.; Okan, S. E.; Aktas, S. *Chem. Pap.* **2020**, *74*, 1881-1889. DOI: <https://doi.org/10.1007/s11696-019-01037-9>.
59. Almeida, M. O.; Barros, D. A. S.; Araujo, S. C.; Faria, S.; Matarollo, V. G.; Honorio, K. M. *Spectrochim. Acta A Mol. Biomol. Spectrosc.* **2017**, *184*, 169-176. DOI: <https://doi.org/10.1016/j.saa.2017.04.070>.
60. Bashaala, A.; Said, M. A.; Assirey, E. A.; Alborki, Z. S.; AlObaid, A. A.; Zarrouk, A.; Warad, I. *J. Mol. Struct.* **2021**, *1238*, 130461. DOI: <https://doi.org/10.1016/j.molstruc.2021.130461>.
61. Kargar, H.; Fallah-Mehrjardi, M.; Behjatmanesh-Ardakani, R.; Munawar, K. S.; Ashfaq, M.; Tahir, M. N. *J. Mol. Struct.* **2022**, *1250*, 131691. DOI: <https://doi.org/10.1016/j.molstruc.2021.131691>.
62. Anwer, K. E.; Sayed, G. H.; Ramadan, R. M. *J. Mol. Struct.* **2022**, *1256*, 132513. DOI: <https://doi.org/10.1016/j.molstruc.2022.132513>.
63. Śmiszek-Lindert, W. E.; Chełmęcka, E.; Lindert, O.; Dudzińska, A.; Kaczmarczyk-Sedlak, I. *Spectrochim. Acta A Mol. Biomol. Spectrosc.* **2018**, *201*, 328-338. DOI: <https://doi.org/10.1016/j.saa.2018.05.021>.
64. Umar, Y. *J. Mol. Struct.* **2022**, 133230. DOI: <https://doi.org/10.1016/j.molstruc.2022.133230>.
65. Unsalan, O.; Szolnoki, B.; Toldy, A.; Marosi, G. *Spectrochim. Acta A Mol. Biomol. Spectrosc.* **2012**, *98*, 110-115. DOI: <https://doi.org/10.1016/j.saa.2012.08.050>.

66. Uluçam, G.; Bagci, U.; Şuekinci Yılmaz, A.; Yentürk, B. *Spectrochim. Acta. A Mol. Biomol. Spectrosc.* **2022**, 279, 121429. DOI: <https://doi.org/10.1016/j.saa.2022.121429>.
67. Mary, Y. S.; Mary, Y. S.; Resmi, K.; Kumar, V. S.; Thomas, R.; Sureshkumar, B. *Heliyon*. **2019**, 5, e02825. DOI: <https://doi.org/10.1016/j.heliyon.2019.e02825>.
68. Daina, A.; Michelin, O.; Zoete, V. *J. Chem. Inf. Model.* **2014**, 54, 3284-3301. DOI: <https://doi.org/10.1021/ci500467k>.
69. Daina, A.; Zoete, V. *Chem. Med. Chem.* **2016**, 11, 1117-21. DOI: <https://doi.org/10.1002/cmdc.201600182>.
70. Walters, W. P.; Murcko, M. A. *Adv. Drug Delivery Rev.* **2002**, 54, 255-71. DOI: [https://doi.org/10.1016/S0169-409X\(02\)00003-0](https://doi.org/10.1016/S0169-409X(02)00003-0).